Thermochimica Acta 481 (2009) 7–11

Contents lists available at ScienceDirect

Thermochimica Acta

journal homepage: www.elsevier.com/locate/tca

Thermodynamic studies on $LnCoO_3(s)$ (Ln = Dy, Ho) by solid-state electrochemical cells

Abhay Patil, Smruti Dash*, S.C. Parida, V. Venugopal

Product Development Section, Bhabha Atomic Research Centre, Trombay, Mumbai 400085, India

ARTICLE INFO

Article history:
Received 8 January 2008
Received in revised form
23 September 2008
Accepted 29 September 2008
Available online 14 October 2008

Keywords:
Rare earth cobalt oxides
Gibbs energy of formation
Thermodynamic functions
Solid electrolyte
Galvanic cell

ABSTRACT

Ternary oxides, $DyCoO_3(s)$ and $HoCoO_3(s)$ have been synthesized by citrate–nitrate gel combustion method and characterized by X-ray powder diffraction method. The standard molar Gibbs energies of formation of $DyCoO_3(s)$ and $HoCoO_3(s)$ have been measured using solid oxide galvanic cell technique employing yttria-stabilized zirconia (YSZ) and calcia-stabilized zirconia (CSZ) as solid electrolyte tubes, respectively. The standard molar Gibbs energies of formation of $DyCoO_3(s)$ and $HoCoO_3(s)$ were calculated from the measured e.m.f. data and are given as:

$$\Delta_f G^\circ_m(DyCoO_3, s, T)\,kJ\,mol^{-1}\ (\pm 4) = -1211.3 + 0.2449^*(T\,K), \quad (1013\,K \le T \ge 1167\,K),$$

$$\Delta_f G^\circ_m(HCoO_3, s, T)\,kJ\,mol^{-1}\ (\pm 4) = -1237.8 + 0.2590^*(T\,K). (964\,K \le T \ge 1102\,K),$$

A set of self consistent thermodynamic functions for $LnCoO_3(s)$ (Ln = La, Nd, Sm, Eu, Gd, Dy, Ho) has been computed from available experimental data in the literature.

1. Introduction

Rare earth cobalt oxides $LnCoO_3(s)$ have potential applications in diverse fields such as in magnetohydrodynamic (MHD) generators [1], oxygen ion conductors [2], catalysts for oxidation of CO [3] and thermoelectric materials [4]. There have been a number of studies on rare earth oxides focusing on its electronic, magnetic, catalytic and thermoelectric properties [5–12], however its thermodynamic properties such as entropy, enthalpy of formation and Gibbs energy of formation have not been systematically studied [13–21]. The successful use of rare earth oxide materials in technical processes requires the knowledge of their thermodynamic stability at high-temperatures, particularly under reducing and oxidizing environments. A set of reliable and consistent thermodynamic data may enable the material scientists to select rare earth ternary oxides for specific technological applications. It is therefore, decided to carry out systematic thermodynamic investigation on these compounds. Recently, present authors [21,23,24] have published results on Gibbs energy of formation of $LnCoO_3(s)$ (Ln = La, Eu, Gd, Tb) and heat capacities of $LnCoO_3(s)$ (Ln = La, Nd, Sm, Eu, Gd, Tb, Dy, Ho). The present work primarily deals with synthesis, characterization of $LnCoO_3(s)$ (Ln = Dy, Ho) and determination of standard molar Gibbs energy of formation of $DyCoO_3(s)$ and $HoCoO_3(s)$ using solid-state electrochemical technique. This study also reports thermodynamic functions for $LnCoO_3(s)$ (Ln = La, Nd, Sm, Eu, Gd, Tb, Dy, Ho), which have been computed from the experimental data.

2. Experimental

2.1. Materials preparation

Ternary oxides, $DyCoO_3(s)$, and $HoCoO_3(s)$ have been synthesized by citrate–nitrate gel combustion route. Preheated $Ln_2O_3(s)$ (Ln = Dy, Ho) (E. Merck, India, mass fraction purity 0.995) and $Co_3O_4(s)$ (STREM Chemicals, USA, mass fraction purity 0.999) with stoichiometric ratios were dissolved in dilute $HNO_3(aq)$. Excess amount of citric acid (E. Merck, India, mass fraction purity 0.999) was added to the solution to assist in complete dissolution. Then pH of the solution was adjusted to 6–7 by adding liquor ammonia. This solution was heated at 450 K, a viscous gel was formed which was dried, crushed in an agate mortar and heated at 1425 K in a platinum crucible for 120 h with two intermediate grindings. The products were identified as $DyCoO_3(s)$ [25] and $HoCoO_3(s)$ [26] by X-ray diffraction (XRD) analysis using a STOE X-ray diffractometer with Cu Kα radiation using graphite monochromator.

Phase mixtures $\{DyCoO_3(s) + Dy_2O_3(s) + CoO(s)\}$, $\{HoCoO_3(s) + Ho_2O_3(s) + CoO(s)\}$ and $\{Ni(s) + NiO(s)\}$ in the molar ratios of 4:2:4,

* Corresponding author. Tel.: +91 22 2559 0648; fax: +91 22 2550 5151.
E-mail address: smruti@barc.gov.in (S. Dash).

0040-6031/$ – see front matter © 2008 Published by Elsevier B.V.
doi:10.1016/j.tca.2008.09.023

4:2:4 and 1:1 respectively, were made using a steel die at a pressure of 100 MPa for the e.m.f. measurements. The {Ni(s) + NiO(s)} pellet was sintered in purified argon gas atmosphere ($p(O_2) \cong 10^{-16}$ kPa) at 1000 K for 7 h. The argon gas was purified by passing it through towers containing the reduced form of BASF catalyst (BASF Aktiengesellschaft, D-6700 Ludwigshafen, Germany), molecular sieves, magnesium perchlorate, and hot uranium metal at 550 K. The {$LnCoO_3$(s) + Ln_2O_3(s) + CoO(s)} pellet was sintered under air at 800 K for 10 h.

2.2. Solid-state electrochemical technique

The experimental details and the cell assembly used for e.m.f. measurements have been reported earlier [27]. A double compartment cell assembly was used. The gas phase over the two electrodes was separated by the use of electrolyte tube so that transport of oxygen from the higher oxygen potential electrode via the gas phase was prevented. The yttria-stabilized zirconia (YSZ) electrolyte tube with 6 mol% Y_2O_3, supplied by Karatec Advanced Materials SA, Spain was used for {$DyCoO_3$(s) + Dy_2O_3(s) + CoO(s)} phase field. The calcia-stabilized zirconia (CSZ) electrolyte tube with 15 mol% calcia, supplied by Nikatto Corporation, Japan was used for {$HoCoO_3$(s) + Ho_2O_3(s) + CoO(s)} phase field. The dimensions of both YSZ and CSZ electrolyte tubes were; 13 mm o.d., 9 mm i.d. and 380 mm long with a flat closed end. Argon gas with different partial pressures of oxygen was flown over the electrodes. An inert environment was maintained over {Ni(s) + NiO(s)} electrode throughout the experiment by streams of purified argon gas ($p(O_2) = 10^{-16}$ kPa). Impure argon gas (bypassing only uranium getter) ($p(O_2)\mu \cong 10^{-4}$ kPa) was flown over {$LnCoO_3$(s) + CoO(s) + Ln_2O_3(s)} (Ln = Dy, Ho) electrode to prevent decomposition of $LnCoO_3$(c) phase at lower oxygen potential. The cell temperature (±1 K) was measured by a calibrated chromel/alumel thermocouple (ITS-90), and the cell e.m.f. (±0.02 mV) by a Keithley 614 electrometer (impedance > 10^{14} Ω). The reversible e.m.f.s of the following solid-state galvanic cells were measured as a function of temperature.

$$\text{Cell(I)} : (-)\text{Pt}/\{\text{Ni(s)} + \text{NiO(s)}\}//\text{YSZ}//\{\text{DyCoO}_3\text{(s)} + \text{Dy}_2\text{O}_3\text{(s)} + \text{CoO(s)}\}/\text{Pt}(+) \quad (1)$$

$$\text{Cell (II)} : (-)\text{Pt}/\{\text{Ni(s)} + \text{NiO(s)}\}//\text{CSZ}//\{\text{HoCoO}_3\text{(s)} + \text{Ho}_2\text{O}_3\text{(s)} + \text{CoO(s)}\}/\text{Pt}\,(+) \quad (2)$$

E.m.f. measurements were carried out in the temperature range of 1000–1200 K. The reversibility of the solid-state electrochemical cells was checked by micro-coulometric titration in both directions. A small quantity of current was passed (~100 μA for ~10 min) through the cell in either direction. The e.m.f. of the cell returned to its original value after the removal of applied voltage. The e.m.f. of cells was also found to be independent of flow rate of the inert gas passing over the electrodes in the range from 120 to 360 $dm^3\,h^{-1}$. E.m.f. values were taken after temperature became constant. At each temperature at least three readings were taken at an interval of 30 min. Then temperature was changed to a desired value and similar procedure was followed. The cell temperature was raised and lowered, alternatively. E.m.f. started drifting after 75 h. Then both electrodes were replaced by previously annealed fresh electrodes. These electrodes were annealed to shorten the equilibrium time. The X-ray diffraction patterns of the {$DyCoO_3$(s) + Dy_2O_3(s) + CoO(s)} and {$HoCoO_3$(s) + Dy_2O_3(s) + CoO(s)} pellets, before and after the experiments are shown in Fig. 1. It shows the presence of $LnCoO_3$(s) [25,26], Ln_2O_3(s) [28,29] and CoO(s) [30] phases and no new phase after the e.m.f. measurements.

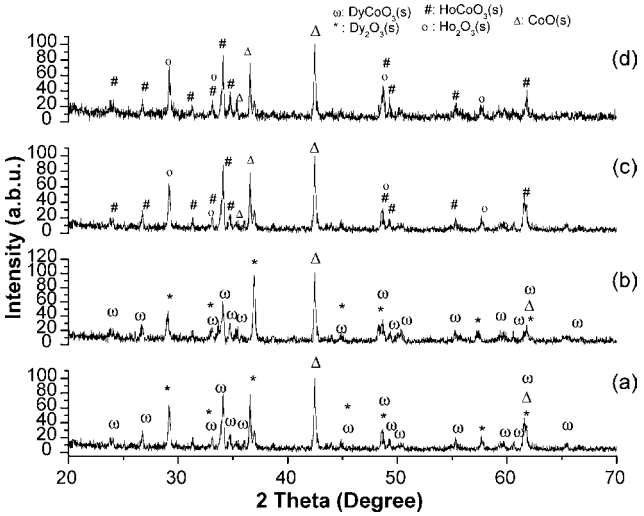

Fig. 1. X-ray diffraction pattern of three phase mixture: {$LnCoO_3$(s) + Ln_2O_3(s) + CoO(s). Intensity (I in arbitrary units) of peaks is plotted against the diffraction angle 2θ (in degrees). The XRD pattern of ($DyCoO_3$(s) + Dy_2O_3(s) + CoO(s)) pellet, before and after the e.m.f. measurements are shown in (a) and (b), respectively. Similarly, (c) and (d) give XRD pattern of ($HoCoO_3$(s) + Ho_2O_3 (s) + CoO(s)) pellet, before and after the e.m.f. measurements.

3. Results

3.1. Solid-state electrochemical measurements

The e.m.f. of the solid oxide galvanic cell is related to the partial pressure of oxygen at the two electrodes by the relation:

$$E = \left(\frac{RT}{nF}\right) \int_{p''(O_2)}^{p'(O_2)} t(O^{2-})\, d\ln p(O_2) \quad (3)$$

where E is the measured e.m.f. of the cell in volts, R (=8.3144 $J\,K^{-1}\,mol^{-1}$) is the universal gas constant, n (=4) is the number of electrons participating in the electrode reaction, F (=96486.4 $C\,mol^{-1}$) is the Faraday constant, T is the absolute temperature, $t(O^{2-})$ is the effective transference number of O^{2-} ion for the solid electrolyte and $p'(O_2)$ and $p''(O_2)$ are the equilibrium oxygen partial pressures at the {$LnCoO_3$(s) (Ln = Dy, Ho) + Ln_2O_3(s) + CoO(s)} and {Ni(s) + NiO(s)} electrodes, respectively. The transference number of oxygen ion in the solid electrolyte used in the present study is nearly unity ($t(O^{2-})$ >0.99) at the oxygen pressures and temperatures covered. Hence, the e.m.f. of the cell is directly proportional to the logarithm of the ratio of partial pressures of oxygen at the electrodes

$$E = \left(\frac{RT}{4F}\right) ln \left\{\frac{p'(O_2)}{p''(O_2)}\right\}. \quad (4)$$

Thus,

$$4FE = \Delta\mu'(O_2) - \Delta\mu''(O_2), \quad (5)$$

where $\mu''(O_2)$ is the oxygen potential over {Ni(s) + NiO(s)}electrode and can be given as:

$$\Delta m''(O_2) = 2\Delta_f G^{\circ}_m(\text{NiO, s}, T). \quad (6)$$

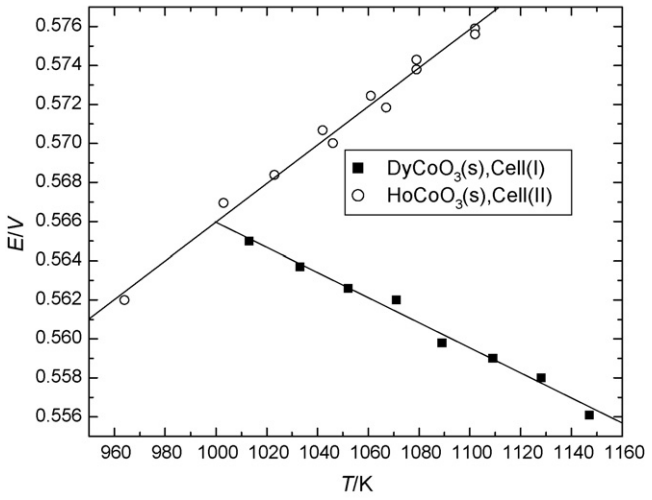

Fig. 2. E.m.f. values of cell(I) and cell(II) as a function of temperature.

$\Delta\mu'(O_2)$ over $\{LnCoO_3(s) + Ln_2O_3(s) + CoO(s)\}$ electrode can be calculated from Eq. (5) and is given as:

$$\Delta\mu'(O_2) = 4FE + 2\Delta_f G^\circ_m(NiO, s, T). \quad (7)$$

$\Delta\mu'(O_2)$ is also related to $\Delta_f G^\circ_m(LnCoO_3, s, T)$ through reaction (8)

$$2Ln_2O_3(s) + 4CoO(s) + O_2(g) = 4LnCoO_3(s) \quad (8)$$

and is given as:

$$\Delta m'(O_2) = 4\Delta_f G^\circ_m(LnCoO_3, s, T) - 4\Delta_f G^\circ_m(CoO, s, T) - 2\Delta_f G^\circ_m(Ln_2O_3, s, T). \quad (9)$$

$\Delta_f G^\circ_m(LnCoO_3, s, T)$ can be calculated from Eqs. (9) and (7) and is given as:

$$\Delta_f G^\circ_m(LnCoO_3, s, T) = FE + 0.5\Delta_f G^\circ_m(NiO, s, T) + \Delta_f G^\circ_m(CoO, s, T) + 0.5\Delta_f G^\circ_m(Ln_2O_3, s, T). \quad (10)$$

3.2. Dy–Co–O system

The variation of the e.m.f. as a function of temperature for cell(I) is shown in Fig. 2 and is given in supplementary data file (Supplementary Table 1). The e.m.f. data were least squares fitted to give the following polynomial:

$$\text{Cell (I)} : E\,(\text{V})(\pm 0.001) = 0.6343 - 6.810 \times 10^{-5} \times T(\text{K}). \quad (11)$$

The oxygen chemical potential over three-phase mixture $\{DyCoO_3(s) + Dy_2O_3(s) + CoO(s)\}$ has been calculated from Eq. (7) and is given as:

$$\Delta\mu(O_2)\,(\text{kJ mol}^{-1})(\pm 1) = -223.6 + 0.1439T\,(\text{K}), \quad (1013\,\text{K} \le T \le 1167\,\text{K}). \quad (12)$$

The standard molar Gibbs energy of formation of $DyCoO_3(s)$ has been calculated from Eq. (10) using e.m.f. values from Eq. (11) and $\Delta_f G^\circ_m(T)$ for $Dy_2O_3(s)$, CoO(s) and NiO(s) from the literature [31,32], given in supplementary data file (Supplementary Table 2). The calculated $\Delta_f G^\circ_m(DyCoO_3, s, T)$ expressions is given as:

$$\Delta_f G^\circ_m(DyCoO_3, s, T)\,(\text{kJ mol}^{-1})(\pm 4) = -1211.3 + 0.2449T\,(\text{K}), \quad (1013\,\text{K} \le T \ge 1167\,\text{K}). \quad (13)$$

$\Delta_f H^\circ_m(DyCoO_3, s, 298.15\,\text{K})$ has been calculated from Eq. (13) using heat capacity values for Dy(s), Co(s) and $O_2(g)$ and their enthalpy of transition and the transition temperature values from the literature [31] and heat capacity of $DyCoO_3(s)$ from our previous study [24]. The calculated $\Delta_f H^\circ_m(DyCoO_3, s, 298.15\,\text{K})$ is $-1262.2\,\text{kJ mol}^{-1}$.

3.3. Ho–Co–O system

The measured e.m.f. values of cell(II) is also given in supplementary data file (Supplementary Table 1) and shown in Fig. 2. The e.m.f. data were least squares fitted to give the following expression:

$$\text{Cell(II)} : E\,(\text{V})(\pm 0.001) = 0.46721 + 9.8821 \times 10^{-5}T\,(\text{K}). \quad (14)$$

The oxygen chemical potential over three-phase mixture: $\{HoCoO_3(s) + Ho_2O_3(s) + CoO(s)\}$ has been calculated from Eq. (7) and is given as:

$$\Delta\mu(O_2)\,(\text{kJ mol}^{-1})\,(\pm 1) = -288.1 + 0.2083T\,(\text{K}), \quad (964\,\text{K} \le T \le 1102\,\text{K}). \quad (15)$$

$\Delta_f G^\circ_m(HoCoO_3, s, T)$ has been calculated from Eq. (10) using e.m.f. values from Eq. (14) and $\Delta_f G^\circ_m(Ho_2O_3, s, T)$ $\Delta_f G^\circ_m(CoO, s, T)$ and $\Delta_f G^\circ_m(NiO, s, T)$ values from the literature [31,32], given in supplementary data file (Supplementary Table 2). The calculated $\Delta_f G^\circ_m(HoCoO_3, s, T)$ expression is given as:

$$\Delta_f G^\circ_m(HoCoO_3, s, T)\,(\text{kJ mol}^{-1})(\pm 4)) = -1237.8 + 0.2590T\,(\text{K}), \quad (964\,\text{K} \le T \le 1102\,\text{K}). \quad (16)$$

Using heat capacity values for Ho(s), Co(s) and $O_2(g)$ and their enthalpy of transition and the transition temperature values from the literature [31] and heat capacity of $HoCoO_3(s)$ from our previous study [24], $\Delta_f H^\circ_m(HoCoO_3, s, 298.15\,\text{K})$ has been calculated from Eq. (16) as $-1268.4\,\text{kJ mol}^{-1}$.

4. Discussion

The standard molar Gibbs energy of formation of $DyCoO_3(s)$ and $HoCO_3(s)$, determined in the present study, is compared with those from literature in supplementary data file (Supplementary Table 2). Petrov et al. [17] have measured the thermodynamic properties of rare-earth cobaltates of $LnCoO_3(s)$ (Ln = Sm, Eu, Gd, Tb, Ho) by employing solid-state electrochemical cells with yttria stabilized zirconia electrolyte in the temperature range of 1074–1488 K. Subasri et al. [22] have measured $\Delta_f G^\circ_m(T)$ for $DyCoO_3(s)$ by e.m.f. technique using yttria stabilized zirconia electrolyte in the temperature range 1080 to 1223 K. The $\Delta_f G^\circ_m(DyCoO_3, s, 1100\,\text{K})$ value ($-941.9\,\text{kJ mol}^{-1}$) calculated from Eq. (13) is in excellent agreement with that ($-941.6\,\text{kJ mol}^{-1}$) of Petrov et al. [17] and that ($-946.4\,\text{kJ mol}^{-1}$) calculated from Subasri et al. [22]. $\Delta_f G^\circ_m(HoCoO_3, s, 1100\,\text{K})$ value ($-952.9\,\text{kJ mol}^{-1}$) calculated from Eq. (16) is matching with that ($-948.5\,\text{kJ mol}^{-1}$) of Petrov et al. [17]. The $\Delta_r G^\circ_m(T)$ values for the cell reaction:

$$0.5Ln_2O_3(s) + CoO(s) + 0.25O_2 = LnCoO_3(s), \quad (Ln = Dy, Ho) \quad (17)$$

have been calculated from Petrov et al. [17], Subasri et al. [22] and present work. These values were plotted as a function of temperature in Fig. 3 which shows reasonable agreement among different measurements.

The oxygen potential diagrams for Dy–Co–O and Ho–Co–O systems have been calculated at 1273 K using FactSage programme

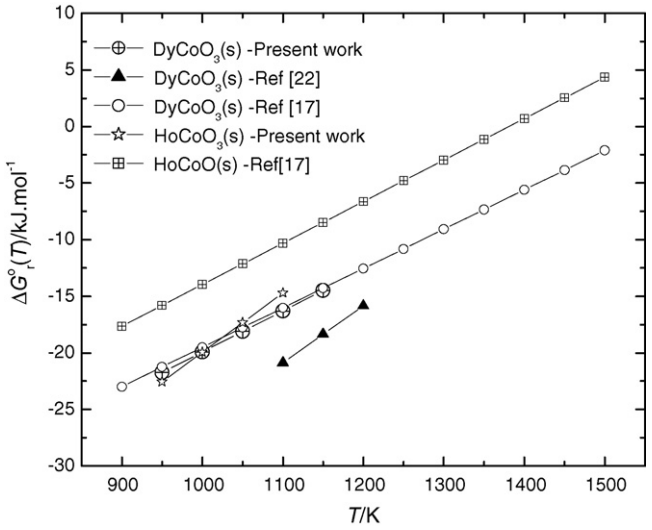

Fig. 3. $\Delta_r G^\circ_m(T)$ values for the reaction: $0.5Ln_2O_3(s) + CoO(s) + 0.25O_2(g) = LnCoO_3(s)$ (Ln = Dy, Ho) have been plotted as a function of temperature. The $\Delta_r G^\circ_m(T)$ values were calculated separately from experimental data of Petrov et al. [17], Subasri et al. [22] and present work.

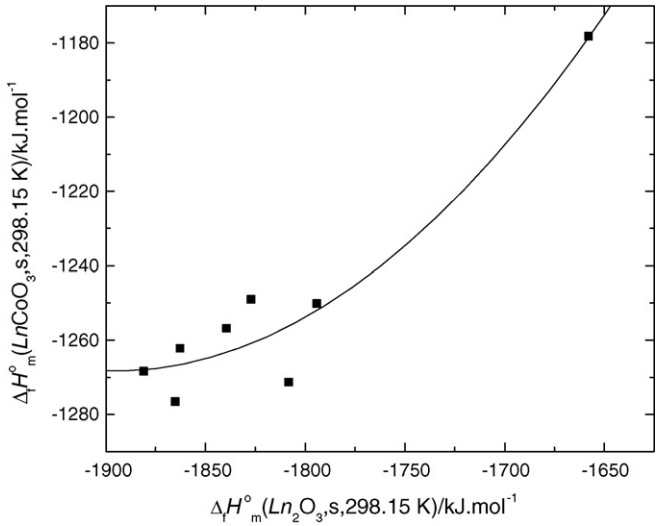

Fig. 5. $\Delta_f H^\circ_m(LnCoO_3, s, 298.15\,K)$ (Ln = La, Nd, Sm, Eu, Gd, Tb, Dy) as a function of $\Delta_f H^\circ_m(Ln_2O_3, s, 298.15\,K)$ values.

[33] and are shown in supplementary data file, respectively. These figures show the stability range of the real phases as a function of $\log p(O_2)$ and the cationic fraction (mole of Co/Co + Ln). It also shows that $LnCoO_3(s)$ compound is stable under higher oxygen potential. The $\Delta_f G^\circ_m(LnCoO_3, s, T)$ (Ln = Dy, Ho) input values for programme were taken from the present study.

The variation of Gibbs energy of formation of $LnCoO_3(s)$ (Ln = La, Nd. Sm, Eu, Gd, Tb, Dy, Ho) with temperature is shown in Fig. 4. The thermodynamic stabilities of $LaCoO_3(s)$ were determined by Sreedharan and Chandrasekharaiah [19,20], Seppanen et al. [16] and Parida et al. [21]. Petrov and co-workers [15,17,18] have reported $\Delta_f G^\circ_m(LnCoO_3, s, T)$ (Ln = La, Nd, Sm, Eu, Gd, Tb, Dy, Ho) using e.m.f. technique in the temperature range 1074–1488 K. Kitayama [13,14] have studied phase equilibria in the system Ln_2O_3–Co–Co_2O_3 (Ln = Nd, Sm, Eu, Gd, Tb) at 1473 K by controlled atmosphere thermogravimetry. Subasri et al. [22] have measured $\Delta_f G^\circ_m(LnCoO_3, s, T)$ (Ln = Nd, Sm, Eu, Gd, Dy) in the temperature range 1100–1200 K and the present authors have measured $\Delta_f G^\circ_m(LnCoO_3, s, T)$ (Ln = La, Sm, Eu, Gd, Tb, Dy, Ho) in the temperature range 1000 to 1200 K. Except Kitayama [13,14], all groups of investigators have employed similar e.m.f. technique. It was found that $\Delta_f G^\circ_m(LnCoO_3, s, T)$ values of various investigators have satisfactory agreement. Hence, present authors have combined data reported by various investigators for each $LnCoO_3(s)$ (Ln = La, Nd, Sm, Eu, Gd, Tb, Dy, Ho) system, separately by least squares analysis method to obtain single Gibbs energy expression in the temperature range 1000–1500 K. The Gibbs energy change for reaction (17) has been calculated for each $LnCoO_3(s)$ (Ln = La, Nd, Sm, Eu, Gd, Tb, Dy, Ho) and is given in supplementary data file (Supplementary Table 3). The Gibbs energy values of $LnCoO_3(s)$ (Ln = La, Nd, Sm, Eu, Gd, Tb, Dy, Ho) system are plotted against temperature in Fig. 4, which shows that $\Delta_f G^\circ_m(LnCoO_3, s, T)$ values are distinctly higher than rest of rare earth cobaltates.

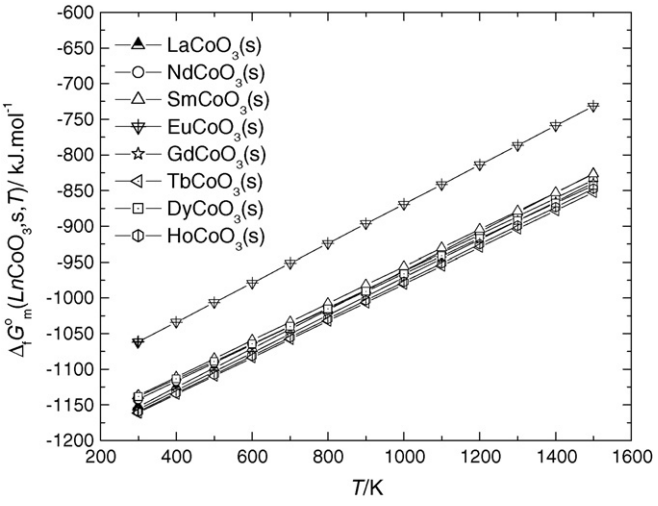

Fig. 4. $\Delta_f G^\circ_m(T)$ ($LnCoO_3, s, T$) (Ln = La, Nd, Sm, Eu, Gd, Tb, Dy, Ho) values as a function of temperature.

Experimental $\Delta_f H^\circ_m(298.15\,K)$ for $LnCoO_3(s)$ have not been reported in the literature. However, present authors have calculated $\Delta_f H^\circ_m(298.15\,K)$ from the reported $\Delta_f G^\circ_m(LnCoO_3, s, T)$ (Ln = La, Nd, Sm, Eu, Gd, Tb) [17,18,21–23], using enthalpy of transition, transition temperature and heat capacity values for Ln(s), Co(s), $O_2(g)$ and $LnCoO_3(s)$ from the literature [24,31]. The calculated $\Delta_f H^\circ_m(298.15\,K)$ values for $LaCoO_3(s)$, $NdCoO_3(s)$, $SmCoO_3(s)$, $EuCoO_3(s)$, $GdCoO_3(s)$, $TbCoO_3(s)$ are −1250.2, −1271.3, −1249.0, −1178.2, −1256.8 and −1276.6 kJ mol^{-1}, respectively. These $\Delta_f H^\circ_m(298.15\,K)$ (Ln = La, Nd, Sm, Eu, Gd, Tb, Dy) values have been plotted against $\Delta_f H^\circ_m(Ln_2O_3, s, 298.15\,K)$ in Fig. 5, from which the present authors have estimated $\Delta_f H^\circ_m(PrCoO_3, s, 298.15\,K)$ as −1254.3 kJ mol^{-1}.

The first order electronic transitions in $LaCoO_3(s)$ [11,16], $NdCoO_3(s)$ [12] and $GdCoO_3(s)$ [12] are reported in the literature. But present authors did not observe any such transition using a Multi detector High Temperature Calorimeter (MHTC-96), supplied by SETARAM instrumentation, France, in its DSC mode. The second order electronic transition temperature and excess electronic entropy of $LnCoO_3(s)$ (Ln = La, Nd, Sm, Eu, Gd, Tb, Dy) are reported in our previous work [24]. These values for $HoCoO_3(s)$ are not reported. The present authors have calculated second order electronic transition temperature for $HoCoO_3(s)$ as 782 K from the plot of transition temperatures of $LnCoO_3(s)$ (Ln = La, Nd, Sm, Eu, Gd, Tb, Dy) as a function of atomic number of rare earth elements. The electronic transition entropy of $HoCoO_3(s)$ is taken same as that for $DyCoO_3(s)$. The $S^\circ_m(298.15\,K)$ values needed for the computation of thermodynamic functions were estimated from

S°_{m}(298.15 K) values of pure CoO(s), Co_3O_4(s) and Ln_2O_3(s) by applying the molar additivity rule and are given in supplementary data file (Supplementary Tables 4–11). Coutures et al. [34] have studied the melting temperature of $LnCoO_3$(s) (Ln= La, Nd, Sm, Gd, Dy, Er, Yb) using thermal analysis technique. The measured melting points for $LaCoO_3$(s), $NdCoO_3$(s), $SmCoO_3$(s), $GdCoO_3$(s), $DyCoO_3$(s), $ErCoO_3$(s), $YbCoO_3$(s) are 2013, 1693, 1613, 1653, 1543, 1493 and 1453 K, respectively. These experimental observations show that $LnCoO_3$(s) are stable up to 1500 K.

Thermodynamic functions such as heat capacity, enthalpy increment, free energy function, entropy, enthalpy, Gibbs energy, enthalpy of formation and Gibbs energy of formations for $LnCoO_3$(s) (Ln = La, Nd, Sm, Eu, Gd, Tb, Dy, Ho) have been computed from 298.15 to 1500 K considering second order transition and absence of first order transition in $LnCoO_3$(s) in this temperature range and results are given in supplementary data file (Supplementary Tables 4–11).

5. Conclusion

The ternary oxides $LnCoO_3$(s), (Ln = Dy, Ho) have been synthesized by citrate–nitrate gel combustion route and characterized by X-ray diffraction method. The oxygen chemical potential, $\Delta\mu(O_2)$ for the three-phase mixture {$LnCoO_3$(s) + Ln_2O_3 (s) + CoO(s)} have been measured by using solid–oxide galvanic cell. The standard molar Gibbs energy of formation of the ternary compound has been calculated from the e.m.f. data and compared with that reported in the literature. Thermodynamic functions for $LnCoO_3$(s) (Ln = La, Nd, Sm, Eu, Gd, Tb, Dy, Ho) have been computed for the first time.

Acknowledgements

The authors are grateful to Dr. Ziley Singh and Mr. B.K. Sen, Head, Product Development Section for their keen interest and constant encouragement during the course of the study. Authors are also thankful to Dr. K. Krishnan of Fuel Chemistry Division for X-ray diffraction analysis.

Appendix A. Supplementary data

Supplementary data associated with this article can be found, in the online version, at doi:10.1016/j.tca.2008.09.023.

References

[1] D.B. Meadowcraft, P.G. Meier, A.C. Warren, Energy Convers. 12 (1972) 145–147.
[2] T.Z. Mazanec, Solid State Ionics, 70/71 (1994) 11.
[3] W.F. Libby, Science 171 (1971) 499.
[4] A. Casalot, P. Dougier, P. Hagenmaller, J. Phys. Chem. Solids 32 (1971) 407.
[5] D.B. Meadowcraft, Nature 226 (1970) 847.
[6] Jiang Lu, Lanying He, Guangyu Chen, Wenhui Su, J. Mater. Sci. 32 (1997) 203.
[7] G. Thornton, F.C. Morrison, S. Partington, B.C. Tofield, D.E. Williams, J. Phys. Solid State Phys. 21 (1988) 2871.
[8] A.N. Jain, S.K. Tiwari, R.N. Singh, P. Chartier, J. Chem. Soc. Faraday Trans. 91 (1995) 1871.
[9] J. Wang, H. Yasuda, K. Inumaru, M. Misono, Bull. Chem. Soc. Jpn. 68 (1995) 1226.
[10] S.C. Sorenson, J.A. Wronkiewicz, L.B. Sis, G.P. Wirtz, Ceram. Bull. 53 (1994) 446.
[11] P.M. Raccah, J.B. Goodenough, Phys. Rev. 155 (1967) 932.
[12] V.G. Bhide, D.S. Rajoria, Y.S. Reddy, G. Rama Rao, G.V. Sobba Rao, C.N.R. Rao, Phys. Rev. Lett. 29 (1972) 1133.
[13] K. Kitayama, J. Solid State Chem. 77 (1988) 366.
[14] K. Kitayama, J. Solid State Chem. 76 (1988) 241.
[15] A.Yu. Kropanev, A.N. Petrov, V.M. Zhukoiski, Russ. J. Inorg. Chem. 28 (1983) 1667.
[16] M. Seppanen, M. Kyto, P. Taskinen, Scand. J. Met. 8 (1979) 199.
[17] A.N. Petrov, A.Yu. Kropanev, V.M. Zhukoiski, Zh. Fiz. Khim. 58 (1984) 50.
[18] A.N. Petrov, V.A. Cherepanov, A.Yu. Zuyev, V.M. Zhukoiski, J. Solid State Chem. 77 (1988) 1.
[19] O.M. Sreedharan, M.S. Chandrasekharaiah, Mater. Res. Bull. 7 (1992) 1135.
[20] O.M. Sreedharan, M.S. Chandrasekharaiah, J. Mater. Sci. 21 (1986) 2581.
[21] S.C. Parida, Ziley Singh, S. Dash, R. Prasad, V. Venugopal, J. Alloys Compd. 285 (1991) 7.
[22] R. Subasri, R. Pankajavalli, O.M. Sreedharan, J. Alloys Compd. 269 (1998) 71.
[23] Abhay Patil, Smruti Dash, S.C. Parida, V. Venugopal, J. Alloys Compd. 384 (2004) 274.
[24] Abhay Patil, Smruti Dash, S.C. Parida, V. Venugopal, Thermochim. Acta 465 (2007) 25.
[25] JCPDS-ICDD file no. 73-1197, PCPDFWIN, Version 2.2, Copyright, 2001.
[26] JCPDS-ICDD file no. 73-1198, PCPDFWIN, Version 2.2, Copyright, 2001.
[27] Z. Singh, S. Dash, R. Prasad, D.D. Sood, J. Alloys Compd. 215 (1994) 303–307.
[28] JCPDS-ICDD file no. 786-1327, PCPDFWIN, Version 2.2, Copyright, 2001.
[29] JCPDS-ICDD file no. 44-1268, PCPDFWIN, Version 2.2, Copyright, 2001.
[30] JCPDS-ICDD file no. 72-1474, PCPDFWIN, Version 2.2, Copyright, 2001.
[31] M. W. Chase Jr., C.A. Davies, J.R. Downey Jr., D. J. Frurip, R.A. McDonald, A.N. Syverud, JANAF Thermochemical Tables, third ed., J. Phys. Chem. Ref. Data 14 (1985).
[32] I. Barin, Thermochemical Data of Pure Substance, third ed., VCH, Weinheim, 1995.
[33] FactSage FactSage, Version 5.4.1, The integrated Thermodynamic Data Bank System, GTT-Technologies, GmbH, Germany, 1976–2006.
[34] J.P. Coutures, J.M. Badie, R. Berjoan, J. Coutures, R. Flamand, A. Rouanet, High Temp. Sci. 13 (1980) 331.